A Composite Joint Sub-aperture Imaging along Nonlinear Trajectories

Wang, Xuan; Krasnov, Oleg; Deng, Jiahao ; Tran, Dihn

DOI
10.1049/cp.2017.0463

Publication date
2018

Document Version
Final published version

Published in
The IET International Conference on Radar Systems 2017

A Composite Joint Sub-aperture Imaging along Nonlinear Trajectories

Xuan Wang[*†], *Oleg Krasnov*[†], *Jiahao Deng*[*], *Dihn Tran*[†]

[*]*School of Mechatronical Engineering, Beijing Institute of Technology, China, X.Wang-5@tudelft.nl*
[†]*Microwave Sensing, Signals and Systems, Delft University of Technology, the Netherlands*

Keywords: Joint Sparsity, Compressive Sensing, Non-linear trajectory, Radar Imaging.

Abstract

In this paper, an imaging algorithm for the airborne radar system maneuvering along an arbitrary trajectory is proposed. The algorithm aims at wide-angle imaging with incomplete measurements from the nonlinear trajectory. The proposed composite joint sub-aperture imaging algorithm provides high reconstruction quality and supports efficient data collection policy. The image can be reconstructed by combining image patches corresponding to non-overlapping sub-apertures. The image patch is obtained by compressive sensing with joint sparse representation of the scene. Numerical results have proved that the proposed algorithm is highly effective and capable of image reconstruction without much loss in quality, especially on objects signature and contour.

1 Introduction

Airborne radar systems are widely used for detection and surveillance in both military and civilian applications. In most cases, the airborne platform trajectory is not ideal linear fight path, especially for small aircrafts or drones flying at low altitude [1]. Such aircrafts are more and more widely used, but do not fly along straight path. Actually, the influence of weather or wind can change the route of these aircrafts. Thus, imaging along non-linear trajectory is a challenging task due to the existence of acceleration and the cross-range-dependent range migration. The geometrical correction should also be taken into account for the imaging along nonlinear trajectories [2]. There are already many researches on the SAR imaging with highly nonlinear trajectories and also the advancements in GPS and INS systems permit collection of corrected data across longer times and arbitrary flight paths [3].

The non-linear trajectory of radar platform often covers a wide angular range, and only limited amount of data can be acquired and stored in practical applications. For a wide angle imaging, the isotropic point scattering model is no longer valid, the angular dependence of scattering amplitude become significant [4]. On the other hand, wide angle imaging offers significant potential advantage for object recognition and visualization, which holds a promise of higher resolution and better information about the scene. In this way, the nonlinear trajectory covering a wide angle can also be wisely utilized with sparsity-driven [5] approach for better imaging performance. In most cases, the imaging along non-linear trajectory can meet the main requirements of a successful Compressive Sensing(CS) reconstruction [6]. In this way, a composite joint sub-aperture imaging algorithm based on CS is proposed in this study for non-linear trajectories.

The outline of this paper is as follows. In Section 2, we analyse the nonlinear trajectories with non-overlapping observation sectors, present the sparse model of the typical ground targets (land-based vehicle). In Section 3, the CS-based imaging algorithm is proposed for sub-aperture and the composition for the whole scene along the nonlinear trajectory. Both the joint sparsity and size of the sub-aperture should be considered. In Section 4, the composite joint sub-aperture imaging results are given and compared with traditional imaging algorithms based on the realistic civilian vehicle datasets. Conclusions and suggestions for future research is presented in Section 5.

2 Sparse Modelling and Scene Description

2.1 Typical Non-linear Trajectory Analysis

A typical case of non-linear trajectory is the circular path (see Fig.1(a)). Another case is a spiral trajectory with a fixed elevation angle shown in Fig.2(a). The Fig.1(b) and Fig.2(b) show the top views of the two trajectories. The azimuth angle region can be divided into N_R observation sectors. For both the circular and spiral trajectories, we get N_R non-overlapping sectors within the 360 region based on azimuth angles .

2.2 Sparsity of the scene

At high frequencies, the electromagnetic scattered fields of the targets with large electrical size can be well modeled by a discrete set of scattering centers. The scattering center model provides a sparse abstraction of complex target scattering. In this research, the land-based vehicle is the only target in the scene observed by an airborne radar sensor at different positions. For a full-aspect target representation, the airborne radar platform moves along a circular trajectory as shown in Fig. 1(a). The

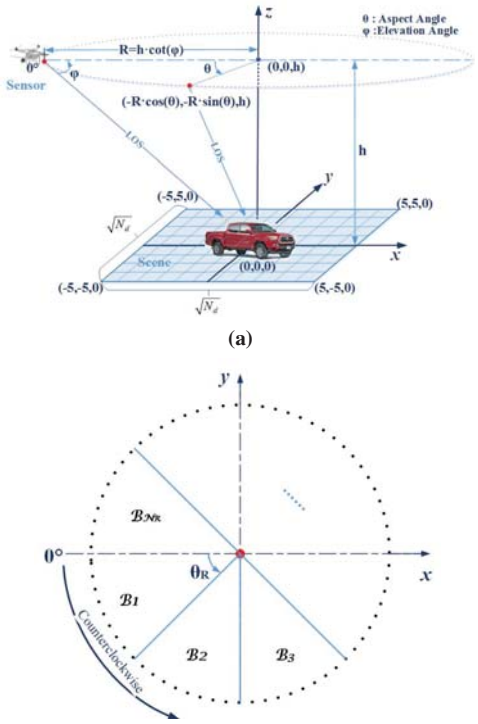

Fig. 1: Typical non-linear trajectories. (a) A circular trajectory;(b) The top view of the circular trajectory.

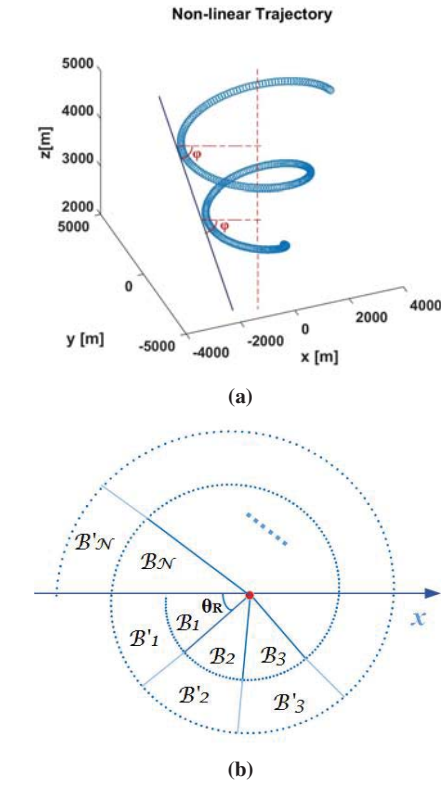

Fig. 2: A typical spiral trajectory. (a) A spiral trajectory with a fixed elevation angle;(b) The top view of the spiral trajectory.

vehicle locates at the center point (0,0,0) of the scene with the size of $6 \times 6m^2$ (see Fig.3).

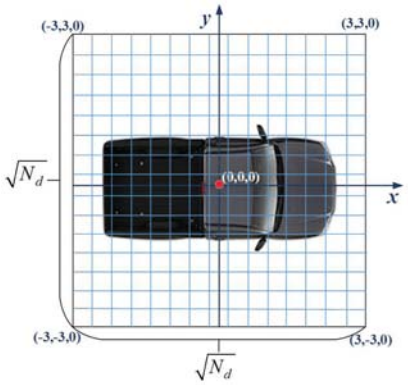

Fig. 3: Discretization of the scene

We discretize the whole scene to N_d scene points. In Fig.3, the scene with a land-based vehicle locating in the center is represented by matrix $\mathbf{X}$ with the size of $M \times M$ ($M = \sqrt{N_d}$ is integer). Since there is only one target of the scene, the matrix X has at most k ($k \ll \sqrt{N_d}$) nonzero rows. We denote $\mathbf{x} = \mathrm{vec}(\mathbf{X}^T), \mathbf{x} \in \mathbb{C}^{N_d}$. So vector $\mathbf{x}$ is sparse with only a few nonzero entries relative to its dimension.

3 CS-based Joint Sub-aperture Imaging

3.1 Compressive Sensing Imaging Algorithm

The compressive sensing(CS) algorithm is exploited for image reconstruction with a reduced number of measurements which are selected randomly. Considering the stepped-frequency signal, the image reconstruction model can be written as:

$$\mathbf{Y} = \mathbf{\Psi}\mathbf{X}, \tag{1}$$

where $\mathbf{\Psi}$ is the sensing matrix. And we denote $\mathbf{y} = \mathrm{vec}(\mathbf{Y}^T) \in \mathbb{C}^{JN_f}$, where J is the number of measurements and N_f is the number of randomly selected frequencies of the transceiver. We denote $\mathbf{A} = \mathbf{\Psi}^T \otimes \mathbf{I} \in \mathbb{C}^{J \times N_d}$, where $\mathbf{A} = \left[\mathbf{A}_1^T, \mathbf{A}_2^T, \ldots, \mathbf{A}_J^T\right]^T$ with $J < N_d$. For the ith transceiver, $\mathbf{A}_i = \exp(-j2\pi \mathbf{f}_i \otimes \boldsymbol{\tau}_i^T) \in \mathbb{C}^{N_f \times N_d}$, where $\mathbf{f}_i = [f_1^i, f_2^i, \ldots, f_{N_f}^i]^T$ represents the randomly selected frequencies and $\boldsymbol{\tau}_i = [\tau_1^i, \tau_2^i, \ldots, \tau_{N_d}^i]^T$ represents the time delays. Then the problem can be transformed into recovering a vector $\mathbf{x} \in \mathbb{C}^{N_d}$ from measurement $\mathbf{y}$,

$$\mathbf{y} = \mathbf{A}\mathbf{x} + \mathbf{m}, \tag{2}$$

where $\mathbf{m}$ represents the noises and clutters contributions of the modeling.

CS-based image reconstruction is to solve the basis pursuit denoise (BP_σ) problem and the least square (LS_τ) problem with the spectral projection gradient ℓ_1-norm (SPGL1) algorithm.

3.2 Imaging for each sub-apertures

For efficient data acquisition and less data storage on board, CS-based algorithm is a good option for image reconstruction. Based on the analysis of observation sectors within the nonlinear trajectory in Section 2.1, we can use the measurements of each observation sectors for the image reconstruction, which is the image patch of the scene.

In order to get better resolution, the image patch is reconstructed for each sub-aperture corresponding to one observation sector. Considering N_R sub-apertures (or observation sectors), we have

$$\mathbf{y}_i = \mathbf{A}_i \mathbf{x}_i + \mathbf{m}, 1 \leq i \leq N_R, \tag{3}$$

where $\mathbf{y}_i$ is the measurement vector in the ith observation sector, and $\mathbf{x}_i$ is the vector of the image patch.

3.3 The composite of the joint sub-aperture for the whole scene

For the same sub-aperture, the scene observed at different aspect angles share a joint sparsity, in the same observation sector, the dominant reflectors of the scene are the same. Assuming that there are totally K measurements for the sub-aperture at different aspect angles, the vector $\mathbf{x}_i^j, 1 \leq j \leq K$ has the same structure of sparsity, while the different vectors $\mathbf{x}_i$ of different observation sectors are different and independent. For the nonlinear trajectory, the observation of the scene changes variously. For providing high spatial resolution, the imaging for each joint sub-aperture can compensate the maneuve ability of the platform. Both the size of the sub-aperture and the maneuvering of the platform should be considered for imaging along the nonlinear path.

The sub-aperture should be wisely designed. For a large sub-aperture covering a wide range of trajectory, the joint sparsity will be weakened due to the maneuvering of the platform. At the same time, the resolution of the image patch will be bad if the sub-aperture is small with less number of measurements. After the reconstruction of image patches as Equation(4), the whole image can be obtained by compositing the image patches.

$$\begin{bmatrix} \mathbf{y}_1 \\ \mathbf{y}_2 \\ \vdots \\ \mathbf{y}_{N_R} \end{bmatrix} = \begin{bmatrix} \mathbf{A}_1 & \mathbf{0} & \dots & \mathbf{0} \\ \mathbf{0} & \mathbf{A}_2 & \dots & \mathbf{0} \\ \vdots & \vdots & \vdots & \vdots \\ \mathbf{0} & \dots & \mathbf{0} & \mathbf{A}_{N_R} \end{bmatrix} \begin{bmatrix} \mathbf{x}_1 \\ \mathbf{x}_2 \\ \vdots \\ \mathbf{x}_{N_R} \end{bmatrix} + \mathbf{m} \tag{4}$$

For the total N_R observation sectors, N_R image patches can be obtained. Then, we can get

$$\mathbf{x} = \sum_{i=1}^{N_R} \mathbf{x}_i, 1 \leq i \leq N_R, \tag{5}$$

where $\mathbf{x}$ is the vector of the image matrix for the whole scene.

4 Numerical Simulation

In this section, we present imaging results based on the civilian vehicle data dome (CV Dome) of a Toyota Tacoma, generated by high-frequency electromagnetic scattering code. The radar database is measured using circular trajectory, which is provided by the Sensor Data Management System [7]. The phase data are collected over 360° azimuths at 30° elevation, with the angular step of 0.0625° and 512 frequency bins within the frequency bandwidth B of 5.35GHz around the center frequency f_c of 9.6GHz. The whole scene is reconstructed as a 210×210 spatial image.

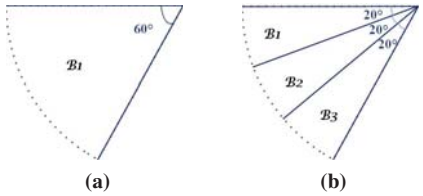

Fig. 4: Discretization of the scene.(a) One obsevation sector of 60°; (b) Three observation sectors of 20°.

First, we choose $N_R = 6$, so the sub-aperture covers 60° angle region (see Fig.4(a)). CS algorithm and Back Projection (BP) algorithm are respectively exploited with randomly chosen 150 frequencies out of 512 and 15% measurements (see Fig. 5). It is clear that the BP is not effective in this case.

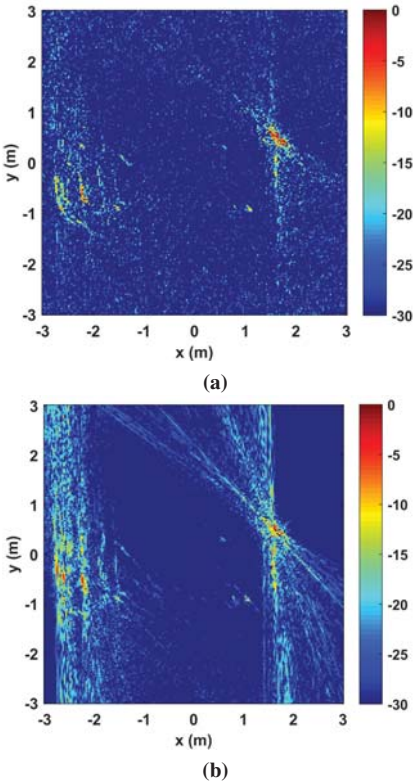

Fig. 5: Imaging results with incomplete dataset for one sub-aperture of 60°.(a) CS imaging; (b) BP imaging.

Then, we choose $N_R = 18$, with sub-aperture covering 20°(see Fig.4(b)). With the same amount of data (150 frequencies out of 512 and 15% measurements), the composite of 3 sub-aperture imaging result of 20° is depicted in Fig.6, which covers the same angle region of 60° with better resolution compared to Fig.5(a).

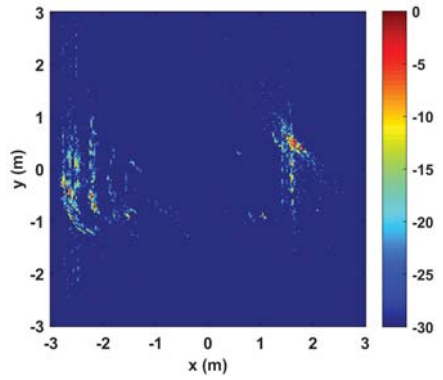

Fig. 6: Composition joint sub-aperture imaging

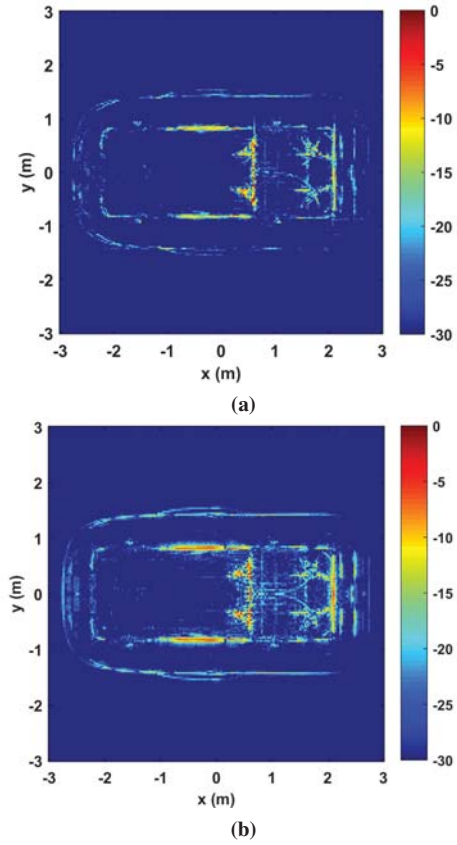

Fig. 7: Imaging results of the whole land-based vehicle.(a) Composition 18 joint sub-apertures imaging result;(b) BP imaging results with full dataset.

The composite image of the whole vehicle is depicted in Fig.7(a), with 18 jointly reconstructed image patches corresponding to the 18 non-overlapping observation sectors. We use BP with the full data set to reconstruct the image of the whole vehicle, which is shown in Fig.7(b). Obviously, the composite result is consistent with the BP result, with much less data used for processing. The composite joint sub-aperture imaging algorithm is also effective for arbitrary trajectories with proper divided observation sectors.

5 Conclusion

A composite joint sub-aperture imaging algorithm is proposed for airborne radar systems flying along nonlinear trajectories. Using joint sparsity of each sub-aperture, a total target image is formed. The incomplete dataset is considered with CS algorithm for efficient data measurement and storage in practical applications. The proposed algorithm is tested on realistic data obtained from CV Dome datasets. Images, resulted from the algorithm proposed, are much sharper than those, which are produced by a classical algorithm. This observed superior performance of the algorithm lays a foundation for many practical applications in the future.

References

[1] O. Frey, C. Magnard, M. Ruegg, and E. Meier. "Focusing of airborne synthetic aperture radar data from highly nonlinear flight tracks", *IEEE Transactions on Geoscience and Remote Sensing*, **47**, pp. 1844-1858, (2009).

[2] Z. Li, M. Xing, Y. Liang, Y. Gao, J. Chen, et al. "A frequency-domain imaging algorithm for highly squinted SAR mounted on maneuvering platforms with nonlinear trajectory", *IEEE Transactions on Geoscience and Remote Sensing*, **54**, pp. 4023-4038, (2016).

[3] R. L. Moses, L. C. Potter, and M. Cetin. "Wide-angle SAR imaging", *Defense and Security*, pp. 164-175, (2004).

[4] I. Stojanovic, M. Cetin, and W. C. Karl. "Joint space aspect reconstruction of wide-angle SAR exploiting sparsity", *SPIE Defense and Security Symposium*, pp. 697005-697005, (2008).

[5] M. Cetin, I. Stojanovic, N. O. Onhon, K. R. Varshney, S. Samadi, et al. "Sparsity-driven synthetic aperture radar imaging: Reconstruction, autofocusing, moving targets, and compressed sensing", *IEEE Signal Processing Magazine*, **31**, pp.27-40, (2014).

[6] L. C. Potter, E. Ertin, J. T. Parker, and M. Cetin. "Sparsity and compressed sensing in radar imaging", *Proceedings of the IEEE*, **98**, pp.1006-1020, (2010).

[7] K. E. Dungan, C. Austin, J. Nehrbass, and L. C. Potter. "Civilian vehicle radar data domes", *SPIE Defense, Security, and Sensing*, **98**, pp.76990P-76990P, (2010).